日本原子力研究開発機構機関リポジトリ

Japan Atomic Energy Agency Institutional Repository

Title	Tolerance of spin-Seebeck thermoelectricity against irradiation by swift heavy ions
Author(s)	Okayasu Satoru, Harii Kazuya, Kobata Masaaki, Yoshii Kenji, Fukuda Tatsuo, Ishida Masahiko, Ieda Junichi, Saito Eiji
Citation	Journal of Applied Physics,128(8), p.083902_1-083902_7
Text Version	Published Journal Article
URL	https://jopss.jaea.go.jp/search/servlet/search?5068931
DOI	https://doi.org/10.1063/5.0014229
Right	This article may be downloaded for personal use only. Any other use requires prior permission of the author and AIP Publishing. This article appeared in Journal of Applied Physics,128(8), p.083902_1-083902_7 and may be found at https://doi.org/10.1063/5.0014229

Satoru Okayasu, Kazuya Harii, Masaaki Kobata, Kenji Yoshii [ID], Tatsuo Fukuda [ID], Masahiko Ishida,
Jun'ichi Ieda [ID], and Eiji Saitoh [ID]

View Online   Export Citation   CrossMark

Tolerance of spin-Seebeck thermoelectricity against irradiation by swift heavy ions

Satoru Okayasu,[1,a)] Kazuya Harii,[1,2] Masaaki Kobata,[3] Kenji Yoshii,[3] Tatsuo Fukuda,[3] Masahiko Ishida,[4] Jun'ichi Ieda,[1,b)] and Eiji Saitoh[1,5,6,7]

AFFILIATIONS

[1]Advanced Science Research Center, Japan Atomic Energy Agency (JAEA), Tokai 319-1195, Japan
[2]Department of Advanced Functional Materials Research, National Institutes for Quantum and Radiological Science and Technology (QST), Takasaki 370-1292, Japan
[3]Materials Sciences Research Center, Japan Atomic Energy Agency, Hyogo 679-5148, Japan
[4]System Platform Research Laboratories, NEC Corporation, Kawasaki 211-8666, Japan
[5]Department of Applied Physics, The University of Tokyo, Tokyo 113-8656, Japan
[6]WPI Advanced Institute for Materials Research, Tohoku University, Sendai 980-8577, Japan
[7]Center for Spintronics Research Network, Tohoku University, Sendai 980-8577, Japan

a)Email address: okayasu.satoru@jaea.go.jp
b)Author to whom correspondence should be addressed: ieda.junichi@jaea.go.jp

ABSTRACT

The ion-irradiation tolerance of thermoelectric devices based on the spin Seebeck effect (SSE) was investigated by using 320 MeV gold ion (Au^{24+}) beams modeling cumulative damages due to fission products emitted from the surface of spent nuclear fuels. For this purpose, prototypical $Pt/Y_3Fe_5O_{12}/Gd_3Ga_5O_{12}$ SSE elements were irradiated with varying the dose level at room temperature and measured the SSE voltage of them. We confirmed that the thermoelectric and magnetic properties of the SSE elements are not affected by the ion-irradiation up to 10^{10} ions/cm^2 fluence and that the SSE signal is extinguished around 10^{12} ions/cm^2, in which the ion tracks almost fully cover the sample surface. We also performed the hard X-ray photoemission spectroscopy (HAXPES) measurements to understand the effects at the interface of $Pt/Y_3Fe_5O_{12}$. The HAXPES measurements suggest that the chemical reaction that diminishes the SSE signals is enhanced with the increase of the irradiation dose. The present study demonstrates that SSE-based devices are applicable to thermoelectric generation even in harsh environments for a long time period.

Published under license by AIP Publishing. https://doi.org/10.1063/5.0014229

I. INTRODUCTION

Spintronics uses both the charge and spin of electrons in solids aiming efficient manipulations and communications in digital data processing.[1–3] On top of that, the spin-conversion capability,[4] i.e., the interconversion among various types of energies via the spin degree of freedom, attracts growing attention since it exhibits a promising pathway to address eager demands for energy harvesting technologies that would power trillion sensors in the forthcoming "Internet of Things (IoT)" society. The discovery of the spin Seebeck effect (SSE)[5–7] opened up such a route offering a new thermoelectric (TE) power generation.[8,9] The SSE is the generation of a spin current

as a result of a temperature gradient in a magnetic material. When a conductor is attached to a magnet and a temperature gradient is applied across the conductor/magnet interface, a spin current induced by the SSE is injected into the conductor and converted into an electrical voltage via the inverse spin Hall effect.

The notable advantage of the spin-driven thermoelectric (STE) generation stems from the orthogonal separation of conventionally coupled heat and charge conduction paths allowing simple and flexible device structures, low-cost fabrication processes, and the unique scaling characteristics of output signals to device dimensions. Large efforts are devoted to enhancing the energy conversion efficiency, which has been tremendously improved in the past

decade,[11–13] and the trend is further propelled with the aid of material informatics using machine learning.[14]

General applications of TE devices span from sensing temperature and heat flow to a waste heat recovery in addition to the aforementioned energy harvesting, depending on heat sources and purposes.[15–17] Furthermore, the potential of the STE devices may be beyond such commoditized uses and is expected workable in more harsh environments, e.g., in the unit of nuclear batteries fueled by radioactive elements and in heat recovery from nuclear wastes. This perspective relies on the fact that, contrary to conventional semiconductor-based electronics, spintronics devices, in general, preclude irradiation damages that may lead to performance degradation as proven in the irradiation tests of magnetic tunneling junctions that consist of metals and oxides[18,19] and even in typical spintronic semiconductors such as n-doped GaAs.[20] While a previous study in fact confirms that a part of the robustness of STE devices is against gamma-ray irradiations of relatively high doses,[21] little knowledge is available for tolerance to other types of irradiation.

In this paper, we investigate the performance of STE devices under heavy ion beam irradiation with varying the dose level. The high energy ions of a heavy element are created as fission products from nuclear wastes stored in dry casks. We model the situation by using swift gold ions with 320 MeV produced by an ion beam accelerator and measure transport properties of the as-irradiated devices with applying temperature gradient. Since the spin-conversion efficiency is largely influenced by the property of the metal/oxide interface of STE devices, we jointly perform hard x-ray photoemission spectroscopy (HAXPES) that clarifies the irradiation effect on the interfacial property. The purpose of this study is to pin down the critical dose level at which the thermoelectric performance of the STE devices dies out. This basic knowledge is indispensable for determining the device service life and for designing a new architecture of thermoelectric-type nuclear batteries based on spintronics technologies.

II. EXPERIMENTAL

The STE sample consists of metallic and magnetic insulator films formed on a substrate.[7] We used Pt and yttrium iron garnet ($Y_3Fe_5O_{12}$, YIG) as the metallic and magnetic insulator layers, respectively. Samples were made by the metal-organic-decomposition (MOD) method[8] based on spin-coating technique. The MOD solution containing the constituent elements (Y and Fe carboxylate dissolved in organic solvents with the chemical composition, Y:Fe = 3:5) are coated on a (111)-oriented single crystal gadolinium gallium garnet ($Gd_3Ga_5O_{12}$, GGG) substrate (500 μm thickness). The spin-coating was set at 500 rpm for 5 s and 1000 rpm for 30 s, followed by a drying step at 150 °C for 3 min. Then, after 500 °C pre-annealing for 5 min, it was annealed at 700 °C for 14 h in the air. We repeat whole the coating and annealing processes again to form a thick crystallized YIG film. Its thickness was estimated to be 200 nm from cross-sectional TEM measurements. After annealing the substrate, the Pt layer was deposited with 5 nm thicknesses on the surface of YIG. For the thermoelectric voltage measurements, the sample was cut into small chips. We confirmed that the sample exhibited the typical SSE output signals.

Next, we performed ion irradiation on the samples with varying the dose level. One sample was set aside as a reference. High energy ion beams were produced at the tandem accelerator in JAEA-Tokai (Japan Atomic Energy Agency, Tokai Research and Development Center) [Fig. 1(a)] where highly collimated and monochromatic ion beams of a variety of ion species from hydrogen (H) to bismuth (Bi) with high energies (~400 MeV by the tandem accelerator alone and ~1000 MeV with the aid of a superconducting booster) and high currents (~3000 nA for H ions and ~10 nA for Au ions) are available. Based on the calculation,[22] we selected gold ions (Au^{24+}) accelerated to the energy 320 MeV that were irradiated on the samples at room temperature. As is well known, when a high energy heavy ion passes through the samples high-density electric excitations occur in semi-conducting or insulating materials.[23,24] For a group of ceramic materials including YIG, columnar defects are formed along the ion tracks if stopping power, S_e, defined as the transfer energies from incident ion to the electron system of the target, exceeds a threshold level (~10 keV/nm).[25] Since the YIG films prepared by the MOD method contain many voids it is hard to visualize the ion-tracks. Instead, typical images of the columnar defects created by Au ion irradiation from the GGG substrate side are shown in Figs. 1(b) and 1(c). These columnar defects are amorphous regions along the incident ion paths with ~20 nm in diameter.[10,26–33] According to the thermal spike model,[34–39] the ion track diameter for amorphizable materials (e.g., YIG) corresponds to the maximum diameter of the transiently molten region. Since the length of the track that depends on the ion energy is calculated as approximately 15 μm for 320 MeV Au ions, ions irradiated from the Pt side penetrate the Pt/YIG layers and end within the GGG substrate. The coverage of an irradiated surface can be estimated by a simple linear model without consideration of overlapping the tracks as a function of ion beam fluence. When irradiation dose exceeds over ~1×10^{12} ions/cm^2, the entire sample surface is covered by the columnar defects. Since amorphous YIG is paramagnetic and does not contribute to the magnon transport at room temperature,[40] the irradiated regions become ineffective for thermoelectric energy conversion via the SSE.

Thermoelectric measurements of the as-irradiated samples were performed at the room temperature using a DC nanovoltmeter and a resistive magnet. The sample properties were evaluated at room temperature using Physical Property Measurement System (PPMS). The Pt/YIG interface of the samples was investigated by HAXPES at the BL22XU in SPring-8.

III. RESULTS

Figure 2(a) shows a change of the output voltage with the Au ion fluence, Φ, varying from $\Phi = 0$–1.4×10^{12} ions/cm^2. The applied temperature difference ΔT between Pt and the substrate that is monitored by two thermocouples is fixed as $\Delta T = 8$ K and the gap between electrodes is 3 mm. The SSE voltage V_{SSE} is estimated by subtracting the saturated voltage value at a negative field from that at a positive field and by dividing the subtracted value by the factor 2. The voltage decreases with the ion fluence, and entirely disappears above the dose of $\Phi = 1 \times 10^{12}$ ions/cm^2 corresponding to that the columnar defects are expected to cover the entire surface of the sample. In Fig. 2(b), the ΔT dependence of the
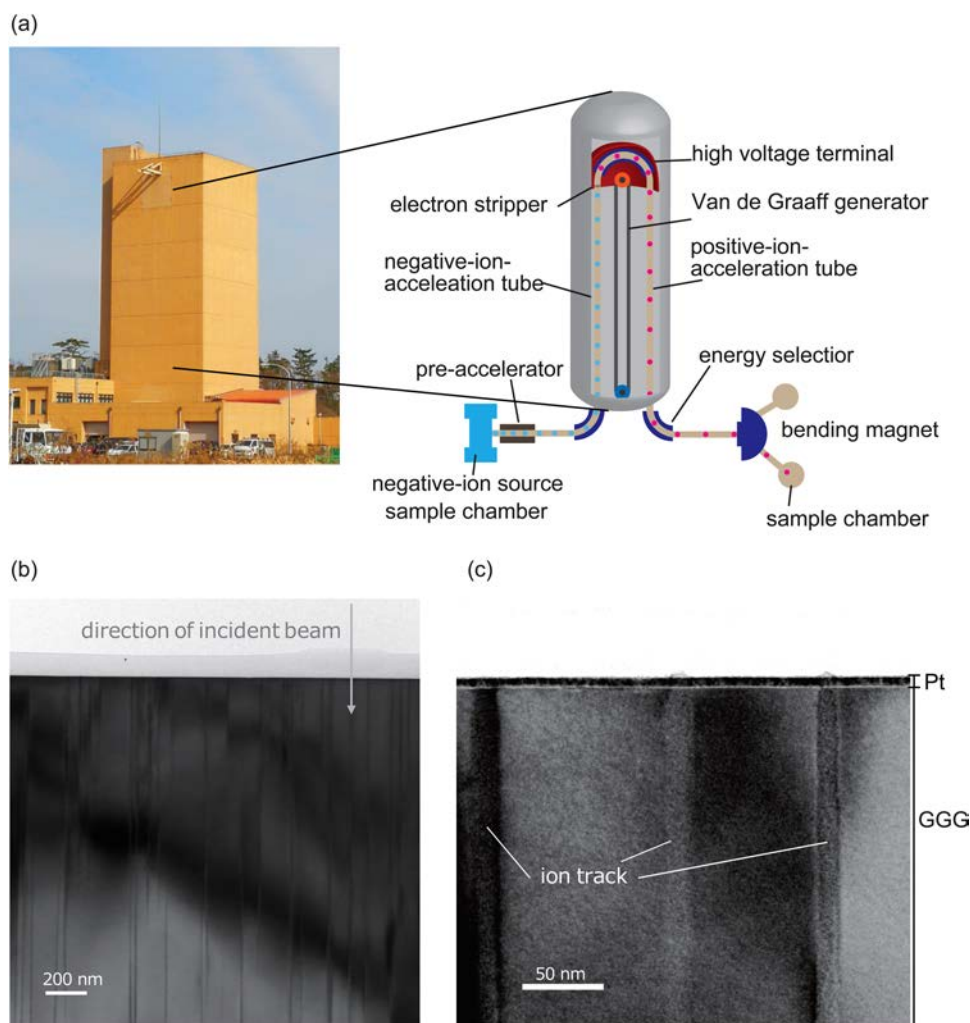
FIG. 1. (a) Schematic view of the tandem accelerator in JAEA-Tokai. The system consists of two-step accelerations of ions with a high voltage terminal. Between the two accelerations, the charge state of ions is transformed from negative to positive ones by passing through an electron stripper (a carbon foil) at the voltage terminal. (b) Bright field image of GGG substrate irradiated with 320 MeV Au^{24+} from the substrate side surface at perpendicular incidence. The direction of the irradiation is indicated by the arrow. (c) Magnified view of the ion tracks created in the irradiated sample.

SSE voltages with the different as-irradiated samples is shown. The linearity of the SSE voltages with ΔT is maintained for all as-irradiated samples suggesting that the decrease of the SSE voltage is a result of an increase of the damaged (amorphized) area of the sample. In Fig. 2(c), the fluence dependence of $V_{\mathrm{SSE}}/\Delta T$ and the calculated coverage ratio of the sample surface by the ion tracks assuming that the track radius is 10 nm are shown. They show the same dependence on the dose.

To understand the origin of the decrease of SSE signals during the ion irradiation process, we evaluate the samples' properties. Resistivity of our Pt/YIG samples does not change by the irradiation, although it is reported that amorphous track overlap increases the resistivity of YIG.[31] Therefore, the metallic Pt layer that governs the sample resistivity is not affected by the irradiation. In our experiment, the change of the sample resistance is ~0.3 % at $\Phi = 1.4 \times 10^{12}$ ions/cm². This is reasonable since the transferred energy to the electron system of the metallic Pt layer by swift ion beams diffuses quickly due to the large electron density in the

metal. On the other hand, the magnetization of the YIG layer is strongly affected by the irradiation. Figure 3(a) shows magnetization hysteresis loops of the samples exhibiting a change of the saturation magnetization with the ion fluence. The behavior is very similar to that of the SSE voltage signals. The fluence dependence of the saturation magnetization is summarized in Fig. 3(b), showing a similar decay as the SSE voltages. This strongly suggests that the decrease of the SSE signal is mainly due to the change of magnetization.

A slight deviation between the measured magnetization and calculated coverage is found in the high fluence region as shown in Fig. 3(b). The SSE voltage in Fig. 2(c) completely disappears above the dose of $\Phi = 1 \times 10^{12}$ ions/cm², while the magnetization in Fig. 3(b) remains finite. The decrease of the SSE voltage with irradiation is mainly caused by the amorphization of YIG, leading to the decrease of the bulk magnetization. In addition, a further reason for the drop for the SSE signal can be attributed to damage to the Pt/YIG interface. To confirm this, we investigate the HAXPES
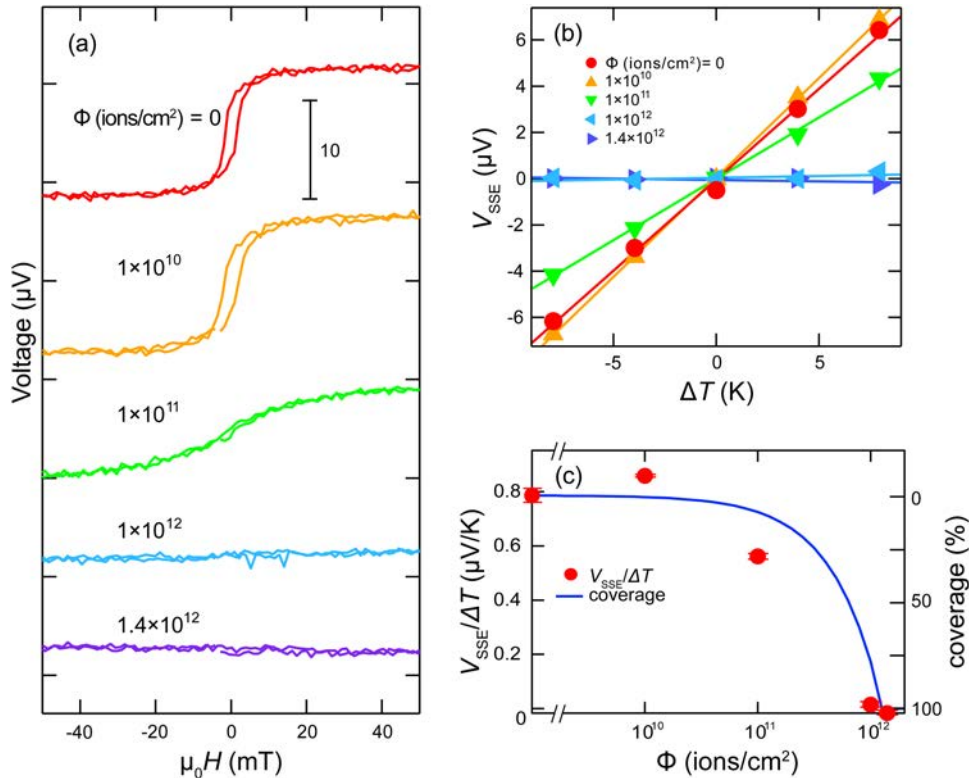
FIG. 2. Measured SSE voltage for the ion-irradiated samples with the fluence, $\Phi = 0$, 1.0×10^{10}, 1.0×10^{11}, 1.0×10^{12}, and 1.4×10^{12} ions/cm^2 (from top to bottom). (a) The output voltage signals as a function of applied magnetic fields from -100 to 100 mT. The temperature difference ΔT between Pt and the substrate is fixed as $\Delta T = 8$ K. (b) The ΔT dependence of the SSE voltages with the different as-irradiated samples. The solid lines are linear fits to the data (symbols). (c) The fluence dependence of the SSE voltages divided by the applied temperature difference, $V_{SSE}/\Delta T$, (filled circles), and the calculated coverage ratio of the sample surface by the ion tracks (solid curve). The error bars mean the standard deviation of the $V_{SSE}/\Delta T$ fittings.

analysis.[41] Since this method offers large probing depths of photoelectrons up to several nanometers with the aid of x-ray energies typically above 5 keV, it has been known as a powerful tool for non-destructive measurements of true bulk states and buried interfaces.[42–44]

The HAXPES measurements were carried out using synchrotron radiation at the beamline BL22XU of SPring-8. The incident x-ray energy was 8 keV. For the HAXPES experiment, we prepared as-irradiated Pt/YIG/GGG samples using single-crystalline 100-nm-thick YIG films. We also carried out the SSE measurements of the as-irradiated SSE devices with this single-crystalline YIG films. The result confirmed the ion-irradiation tolerance of the SSE devices was kept for the single-crystalline YIG. The detailed comparison will be discussed elsewhere. The various photoelectron peaks such as Fe 1s, Fe 2p, O 1s, Pt 4f, and Y 3d were measured at room temperature. The other experimental details have been noted elsewhere.[45] Figure 3(c) shows HAXPES spectra in the O 1s region for various dose levels. The binding energies become monotonically larger with the increase of the irradiation dose as shown in Fig. 3(d). The small peak that appears in the higher energy for as-irradiated samples grows with the Au ion dose suggesting that it originates from the oxygen deficiency in YIG. The binding energies of Fe 2$p_{3/2}$ show similar behavior, but those of Pt 4f do not change. This tendency has been demonstrated previously at Pt/YIG interfaces[41] probing an occurrence of the interfacial chemical reaction due to sputtering damages. The same tendency observed in the present measurements indicates that the interface chemical reaction might be enhanced by the ion beam irradiation.

IV. DISCUSSION

In this work, we find that the SSE signal maintains against the high energy heavy ion irradiation up to the dose of $\Phi = 1 \times 10^{10}$ ions/cm^2, and it vanishes for 1×10^{12} ions/cm^2 due to the damages on the YIG layer of the SSE element. The results show that the STE devices are tolerant of the single event effects as similar to conventional TE devices. On the other hand, cumulative damages due to the ion irradiation limit the workable time period of the STE device if one uses it for nuclear batteries where the SSE element is directly coupled, without shielding, to the radiative element that emits high energy fission products.

We first examine the case that plutonium-238 (^{238}Pu) is used as the radioisotope heat source. In fact, ^{238}Pu has been commonly used for TE nuclear batteries based on conventional TE technologies since it only emits a 5 MeV alpha ray in the decay process that can be easily shielded. Using the SRIM code,[22] the damages by the 5 MeV alpha particles on the thin layer of a Pt(5 nm)/YIG (100 nm)/GGG(30 μm) stacking were estimated. The average damage rate in the YIG layer is 2.4×10^{-4} (Å ions)$^{-1}$, and the displacement per atom (dpa) is 5.76×10^{-6}. On the other hand, the average damage by 320 MeV Au ions is 6.4×10^{-2} (Å ions)$^{-1}$, and the dpa is 1.54×10^{-3}. If we simply compare the impacts between
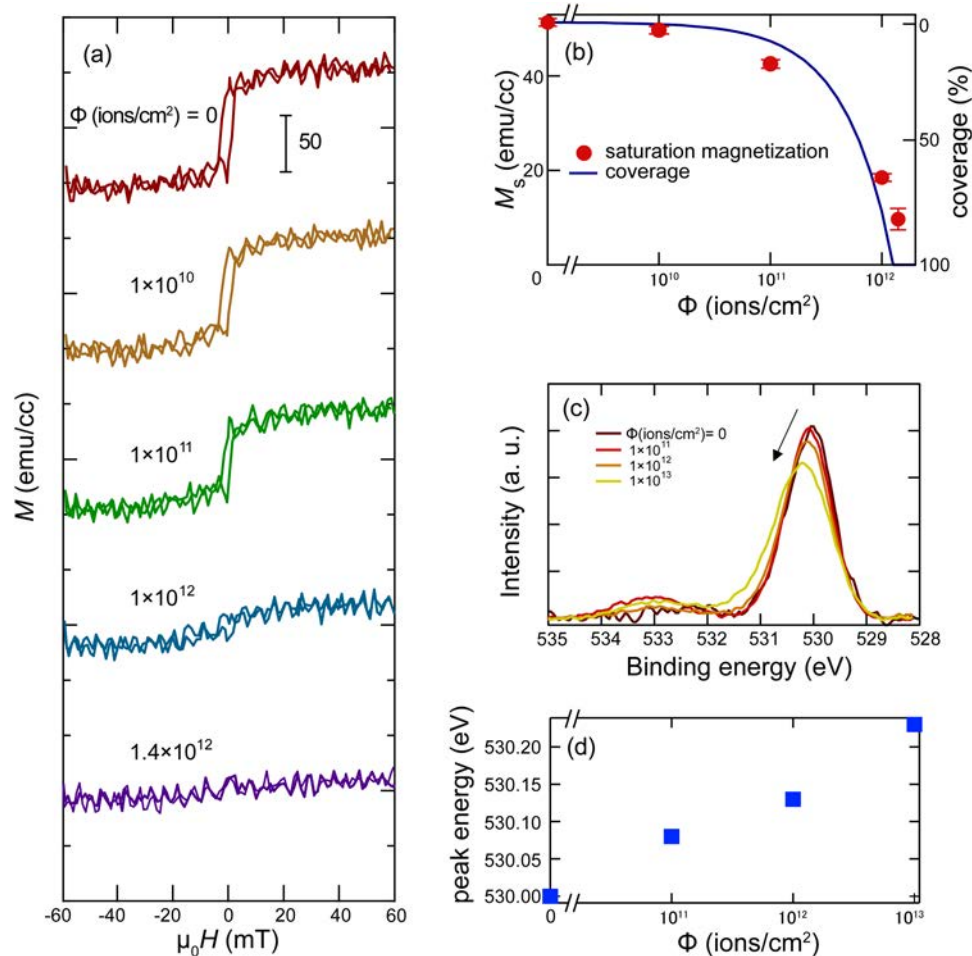
FIG. 3. Measured magnetization and HAXPES for the ion-irradiated samples with the fluence, $\Phi = 0$, 1.0×10^{10}, 1.0×10^{11}, 1.0×10^{12}, and 1.4×10^{12} ions/cm^2 (from top to bottom). (a) The magnetization vs applied magnetic fields from -100 to 100 mT. (b) The fluence dependence of the saturation magnetization (filled circles) and the calculated coverage ratio of the sample surface by the ion tracks (solid curve). The error bars mean the standard deviation of the magnetization fittings. (c) HAXPES spectra in the O $1s$ region for various dose levels. (d) The fluence dependence of the peak energies taken from the HAXPES.

the alpha particle and the heavy ion irradiation by the dpa values, the device exhibits about 300 times tolerant against the former than the latter.

Next, we evaluate the high energy ion flux at the surface of a spent nuclear fuel (SNF). We consider a SNF with high burnup that contains fissile materials such as uranium-235 (^{235}U) and ^{239}Pu stored in a dry cask (5.5 m in height and 2.4 m in diameter). Those elements exhibit nuclear fission when they absorb thermal neutrons (the kinetic energy <1 eV) producing high energy neutrons and fission fragments. According to the measured dose of neutrons at the surface of the dry cask $\sim 5 \times 10^9$ n/s[46] that counts essentially all the nuclear fission processes, regardless of whether it originates in a nuclear reaction or a radioactive decay, we may roughly estimate the upper-bound of the creation rate of fission products in the SNF to be the same order or less. Since the projected range for heavy ions with the kinetic energy ~ 100 MeV in materials is about $10\,\mu$m that is extremely shorter than that of neutrons, only ions created at the vicinity of the surface can be emitted from the SNF, yielding the maximum flux of the fission fragments ~ 0.2 ions/cm^2/s. This crude estimate in conjunction with our

observation already assures that the STE devices work for more than several hundred years around SNFs without degradation. Obviously, if ones attach the substrate side of STE devices to a radioisotope heat source by sacrificing the efficiency of heat energy recovery, the YIG layer can be protected from the ion irradiation effect.

V. CONCLUSIONS

In summary, we have investigated the ion-irradiation tolerance of spin-driven thermoelectric (STE) devices powered by the spin Seebeck effect (SSE). Using swift 320 MeV gold ion beams with several dose levels for the irradiation tests of the devices at room temperature that simulate a harsh environment near dry casks of nuclear wastes, we have confirmed that the thermoelectric and magnetic properties of the STE devices are maintained against the ion-irradiation up to 10^{10} ions/cm^2 fluence and found that the critical fluence at which the SSE signal completely vanishes is around 10^{12} ions/cm^2 fluence. At that dose level, on the other hand, the bulk magnetization of the samples remains still finite. We consider

that the reason for the signal dying out even in the finite magnetization remaining might be the surface chemical reaction facilitated by the high dose level ion-irradiation based on the hard x-ray photoemission spectroscopy (HAXPES) measurements. This basic knowledge is indispensable for determining the device service life in designing a new architecture of thermoelectric-type nuclear batteries based on spintronics technologies. Our findings encourage the use of STE devices applicable to thermoelectric generation even in highly radiative harsh environments for a reasonable time period.

DATA AVAILABILITY

The data that support the findings of this study are available from the corresponding authors upon reasonable request.

REFERENCES

[1]*Spin Current*, 2nd ed., edited by S. Maekawa, S. O. Valenzuela, E. Saitoh, and T. Kimura (Oxford University Press, Oxford, 2017).

[2]B. Dieny *et al.*, "The SpinTronicFactory roadmap: A European community view," SciTech Europa Q. **30**, 114 (2019); available at https://www.scitecheuropa.eu/spintronicfactory-roadmap/93307/.

[3]A. Hirohata, K. Yamada, Y. Nakatani, L. Prejbeanu, B. Diény, P. Pirro, and B. Hillebrands, "Review on spintronics: Principles and device applications," J. Magn. Magn. Mater. **509**, 166711 (2020).

[4]Y. Otani, M. Shiraishi, A. Oiwa, E. Saitoh, and S. Murakami, "Spin conversion on the nanoscale," Nat. Phys. **13**, 829 (2017).

[5]K.-I. Uchida *et al.*, "Observation of the spin-Seebeck effect," Nature **455**, 778 (2008).

[6]K.-I. Uchida *et al.*, "Spin Seebeck insulator," Nat. Mater. **9**, 894 (2010).

[7]K.-I. Uchida, H. Adachi, T. Ota, H. Nakayama *et al.*, "Observation of longitudinal spin-Seebeck effect in magnetic insulators," Appl. Phys. Lett. **97**, 172505 (2010).

[8]A. Kirihara *et al.*, "Spin-current-driven thermoelectric coating," Nat. Mater. **11**, 686 (2012).

[9]K.-I. Uchida *et al.*, "Thermoelectric generation based on spin seebeck effects," Proc. IEEE **104**, 1946 (2016).

[10]J.-M. Costantini, J. M. Desvignes, and M. Toulemonde, "Amorphization and recrystallization of yttrium iron garnet under swift heavy ion beams," J. Appl. Phys. **87**, 4164 (2000).

[11]R. Ramos *et al.*, "Unconventional scaling and significant enhancement of the spin Seebeck effect in multilayers," Phys. Rev. B **92**, 220407(R) (2015).

[12]J. B. S. Mendes, R. O. Cunha, O. Alves Santos, P. R. T. Ribeiro, F. L. A. Machado, R. L. Rodríguez-Suárez, A. Azevedo, and S. M. Rezende,

[13] "Large inverse spin Hall effect in the antiferromagnetic metal $Ir_{20}Mn_{80}$," Phys. Rev. B **89**, 140406(R) (2014).

[14]K.-D. Lee *et al.*, "Thermoelectric signal enhancement by reconciling the spin Seebeck and anomalous nernst effects in ferromagnet/non-magnet multilayers," Sci. Rep. **5**, 10249 (2015).

[14]Y. Iwasaki *et al.*, "Machine-learning guided discovery of a new thermoelectric material," Sci. Rep. **9**, 2751 (2019).

[15]D. M. Rowe, *CRC Handbook of Thermoelectrics: Macro to Nano* (CRC Press, 2005).

[16]H. J. Goldsmid, *Introduction to Thermoelectricity* (Springer, 2010).

[17]L. E. Bell, "Cooling, heating, generating power, and recovering waste heat with thermoelectric systems," Science **321**, 1457 (2008).

[18]H. Hughes *et al.*, "Radiation studies of spin-transfer torque materials and devices," IEEE Trans. Nucl. Sci. **59**, 3027 (2012).

[19]D. Kobayashi *et al.*, "Influence of heavy ion irradiation on perpendicular-anisotropy CoFeB-MgO magnetic tunnel junctions," IEEE Trans. Nucl. Sci. **61**, 1710 (2014).

[20]B. C. Pursley *et al.*, "Robustness of n-GaAs carrier spin properties to 5 MeV proton irradiation," Appl. Phys. Lett. **106**, 072403 (2015).

[21]A. Yagmur *et al.*, "Gamma radiation resistance of spin Seebeck devices," Appl. Phys. Lett. **109**, 243902 (2016).

[22]J. F. Ziegler, see http://www.srim.org/ for "The Stopping and Range of Ions in Matter. SRIM-2013" (2013).

[23]K. Izui, "Fission fragment damage in semiconductors and ionic crystals," J. Phys. Soc. Jpn. **20**, 915 (1965).

[24]A. Tonomura, H. Kasai, O. Kamimura, T. Matsuda, K. Harada, Y. Nakayama, J. Shimoyama, K. Kishio, T. Hanaguri, K. Kitazawa, M. Sasase, and S. Okayasu, "Observation of individual vortices trapped along columnar defects in high-temperature superconductors", Nature **412**, 620 (2001).

[25]*Ion Beam Modification of Solids*, edited by W. Wesch and E. Wendler (Springer International Publishing, 2016).

[26]A. Meftah, F. Brisard, J. M. Costantini, M. Hage-Ali, J. P. Stoquert, F. Studer, and M. Toulemonde, "Swift heavy ions in magnetic insulators: A damage-cross-section velocity effect," Phys. Rev. B **48**, 920 (1993).

[27]J. Jensen, A. Dunlop, S. Della-Negra, and M. Toulemonde, "A comparison between tracks created by high energy mono-atomic and cluster ions in $Y_3Fe_5O_{12}$," Nucl. Instrum. Methods Phys. Res. B **146**, 412 (1998).

[28]J. M. Costantini, F. Brisard, L. Autissier, M. Caput, and F. Ravel, "Study of the amorphization of ion-irradiated yttrium iron garnet by high-resolution diffraction techniques," J. Phys. D Appl. Phys. **26**, A57 (1993).

[29]J. M. Costantini, J. M. Desvignes, A. Pérez, and F. Studer, "Local order and magnetic behavior of amorphous and nanocrystalline yttrium iron garnet produced by swift heavy ion irradiations," J. Appl. Phys. **87**, 1899 (2000).

[30]J. M. Costantini, F. Studer, and J. C. Peuzin, "Modifications of the magnetic properties of ferrites by swift heavy ion irradiations," J. Appl. Phys. **90**, 126 (2001).

[31]J. M. Costantini, S. Miro, F. Beuneu, and M. Toulemonde, "Swift heavy ion-beam induced amorphization and recrystallization of yttrium iron garnet," J. Phys. Condens. Matter **27**, 496001 (2015).

[32]N. Ishikawa, T. Taguchi, and N. Okubo, "Hillocks created for amorphizable and non-amorphizable ceramics irradiated with swift heavy ions: TEM study," Nanotechnology **28**, 445708 (2017).

[33]N. Ishikawa, T. Taguchi, A. Kitamura, G. Szenes, M. E. Toimil-Molares, and C. Trautmann, "TEM analysis of ion tracks and hillocks produced by swift heavy ions of different velocities in $Y_3Fe_5O_{12}$," J. Appl. Phys. **127**, 055902 (2020).

[34]M. Toulemonde and F. Studer, "Comparison of the radii of latent tracks induced by high-energy heavy ions in $Y_3Fe_5O_{12}$ by HREM, channelling Rutherford backscattering and Mössbauer spectrometry," Philos. Mag. **58**, 799 (1988).

[35]M. Toulemonde, "Nanometric phase transformation of oxide materials under GeV energy heavy ion irradiation," Nucl. Instrum. Methods Phys. Res. B **156**, 1 (1999).

[36]G. Szenes, "Monoatomic and cluster ion irradiation induced amorphous tracks in yttrium iron garnet," Nucl. Instrum. Methods Phys. Res. B **146**, 420 (1998).

[37]G. Szenes, "Ion-velocity-dependent track formation in yttrium iron garnet: A thermal-spike analysis," Phys. Rev. B **52**, 6154 (1995).

[38]M. Sasase *et al.*, *Advances in Superconductivity XII* (Springer Japan, Tokyo, 2000), p. 314.

[39]S. Okayasu *et al.*, "Irradiation effects on MgB_2 bulk samples and formation of columnar defects in high-Tc superconductor," Physica C **382**, 104 (2002).

[40]J. M. Gomez-Perez *et al.*, "Absence of evidence of spin transport through amorphous $Y_3Fe_5O_{12}$," Appl. Phys. Lett. **116**, 032401 (2020).

[41]M. Kobata *et al.*, "Hard X-ray photoelectron spectroscopy study of Pt/$Y_3Fe_5O_{12}$," JPS Conf. Proc. **30**, 011192 (2020).

[42]E. Ikenaga *et al.*, "Interface reaction of poly-Si/high-k insulator systems studied by hard X-ray photoemission spectroscopy," J. Electron Spectrosc. Relat. Phenom. **144–147**, 491 (2005).

[43]C. Zborowski *et al.*, "Quantitative determination of elemental diffusion from deeply buried layers by photoelectron spectroscopy," J. Appl. Phys. **124**, 085115 (2018).

[44]G. Conti *et al.*, "Characterization of free-standing InAs quantum membranes by standing wave hard x-ray photoemission spectroscopy," APL Mater. **6**, 058101 (2018).

[45]M. Kobata *et al.*, "Chemical form analysis of reaction products in Cs-adsorption on stainless steel by means of HAXPES and SEM/EDX," J. Nucl. Mater. **498**, 387 (2018).

[46]H. S. Suárez, F. Becker, A. Klix, B. Pang, and T. Döring, "Neutron flux measurements on a mock-up of a storage cask for high-level nuclear waste using 2.5 MeV neutrons," J. Radiol. Prot. **38**, 881 (2018).